water

MDPI

Article

A New Look at Storm Separation Technique in Estimation of Probable Maximum Precipitation in Mountainous Areas

Yifan Liao [1,2], Bingzhang Lin [2,*], Xiaoyang Chen [3] and Hui Ding [1,2]

[1] School of Atmospheric Science, Nanjing University of Information Science and Technology, Nanjing 210044, China; lyifan322@163.com (Y.L.); dinghui_09@nuist.edu.cn (H.D.)
[2] Applied Hydrometeorological Research Institute, Nanjing University of Information Science and Technology, Nanjing 210044, China
[3] Meteorological Bureau of Shaoguan City, Shaoguan 512028, China; cxy921020@126.com
* Correspondence: lbz@nuist.edu.cn

Received: 11 March 2020; Accepted: 14 April 2020; Published: 20 April 2020

Abstract: Storm separation is a key step when carrying out storm transposition analysis for Probable Maximum Precipitation (PMP) estimation in mountainous areas. The World Meteorological Organization (WMO) has recommended the step-duration-orographic-intensification-factor (SDOIF) method since 2009 as an effective storm separation technique to identify the amounts of precipitation caused by topography from those caused by atmospheric dynamics. The orographic intensification factors (OIFs) are usually developed based on annual maximum rainfall series under such assumption that the mechanism of annual maximum rainfalls is close to that of the PMP-level rainfall. In this paper, an alternative storm separation technique using rainfall quantiles, instead of annual maximum rainfalls, with rare return periods estimated via Regional L-moments Analysis (RLMA) to calculate the OIFs is proposed. Based on Taiwan's historical 4- and 24-h precipitation data, comparisons of the OIFs obtained from annual maximum rainfalls with that from extreme rainfall quantiles at different return periods, as well as the PMP estimates of Hong Kong from transposing the different corresponding separated nonorographic rainfalls, were conducted. The results show that the OIFs obtained from rainfall quantiles with certain rare probabilities are more stable and reasonable in terms of stability and spatial distribution pattern.

Keywords: Probable Maximum Precipitation (PMP); storm separation technique; step-duration-orographic-intensification-factor (SDOIF) method; Regional L-moments Analysis (RLMA)

1. Introduction

The Probable Maximum Precipitation (PMP) is defined by the World Meteorological Organization (WMO) as "the greatest depth of precipitation for a given duration meteorologically possible for a design watershed or a given storm area at a particular location at a particular time of year, with no allowance made for long-term climatic trends" [1]. Typically, PMP is required for assessing the Probable Maximum Flood (PMF) which is used to design dam spillways in order to minimize the loss of life and damage to property due to the failure or overtopping of the dam wall under flood [2,3]. PMF may also be applied to define the extent of floodplain areas at risk in extreme flood conditions [2,4]. With the increasing frequency of hydrometeorological extreme events in recent decades, there has been a growing need for more reliable estimates of PMP.

The WMO gives the following six methods that are currently used to estimate PMP [1]: (a) local storm maximization; (b) storm transposition; (c) temporal and spatial maximization of storm; (d)

theoretical model; (e) generalized estimation; (f) statistical estimation. These methods are not totally independent and could be combined. Methods (a)–(e) can be categorized as a hydrometeorological or a causal approach in which the PMP is mainly determined by maximization or transposition of major historical rainstorms [1,5]. Method (c) is a technical treatment depending upon the data availability while method (e) is generalized estimation based on the methods (a)–(c) for a large area. Method (d) is a physical-based method of either convergence model or laminar model and less adopted in practice because of instable results due to less knowledge on extreme storm physics and lack of wind field data of upper meteorology as well. Method (f) is a quasi-statistical approach where the estimation of PMP is derived from a modified frequency analysis of the annual maximum rainfall data or the rainfall quantiles [1,5].

Storm transposition is widely used by practitioners as a means of incorporating additional information about precipitation events from nearby locations to design areas where high efficiency storms are rare and sometimes lacking [1]. In mountainous regions, the transposition areas are usually restricted to those places where the topographic and meteorological characteristics are similar to those at the place where the storm occurred [1]. To expand the transposable regions, storm separation method is applied, through which the mountainous storm rainfall can be separated into two components: that caused by the movement of precipitation weather systems, called convergence component or convergence rain; and that caused by orographic effects, called orographic component or orographic rain [1]. Then, the convergence component could be transposed in a larger area and may be combined with the local orographic component at the design area to form PMP estimates. Therefore, the main difficulty of this method consists in quantitatively expressing the effects of orography on rainfall. The step-duration-orographic-intensification-factor (SDOIF) method, developed by Lin [6,7] and recommended by WMO in Manual on Estimation of PMP [1], is an effective storm separation technique. It is a combined engineering hydrologic-meteorological and geomorphological approach based on long-term rainfall statistics, synoptic analysis of storms and topographic features in a gridded design area. In this method, annual maximum rainfall data are usually used to calculate the orographic intensification factors (OIFs) under the assumption that the formation mechanism of heavy rainstorms approach that of the PMP-level storms. Zhang and Chen [8] adopted the SDOIF method to identify the convergence component of maximum 24-h rainfall of Typhoon Morakot over Taiwan during 8–10 August 2009, then transposed it to Hong Kong for PMP study. Furthermore, taking into account that PMP is an extra-extreme event, the design storms with long recurrence should be closer to PMP in terms of storm mechanism and can be considered as the input data instead of the annual maximum rainfalls to compute the OIFs. In this procedure, reliable rainfall frequency estimates should be obtained prior to computation of the OIFs.

Generally, there are two approaches to perform the frequency analysis of extreme events, at-site and regional. Since at-site frequency analysis needs a collection of long periods of records, the reliability of estimates is usually hampered by the lack of observation networks and insufficient length of recorded data, especially when estimating events of large return periods [9]. In this regard, alternatively, a regional frequency analysis is applied to supplement the limited sample size by incorporating spatial data from several sites having similar characteristics in a homogeneous region, which can improve the quality of the quantile estimates by reducing the uncertainties of the quantiles [10]. The index-flood method is one of the most widely used regionalization approaches. It arose early for flood data analysis in hydrology [11] but can be applied to any kind of variable now [10]. Hosking and Wallis [12] proposed an index-flood procedure, which makes the assumption that the sites' flood frequency distributions in a homogeneous region are identical apart from a scale parameter. It was used with L-moments approach to undertake regional flood frequency analysis [12]. Later, by applying the concept of regional analysis, Lin et al. separated a rainfall into two components, common component and local component, in the practices of precipitation frequency analysis for the NOAA Atlas 14 in the U.S. [13–15] as well as for the Taihu Lake Basin in China [15,16]. He suggested that the regional analysis is more appropriate for precipitation frequency analysis than for flood (flow discharge) frequency analysis because there is

less interdependency among rainfall data at sites than flood data in a homogenous region. Furthermore, combining the regional analysis with the L-moments to form the regional L-moments precipitation frequency approach that performs precipitation frequency analysis can get quantiles that are both more precise in terms of parameter estimation and more reliable in terms of accuracy of quantiles [13,15,16]. It is reported that L-moments have the theoretical advantages over conventional moments of being more robust to the presence of outliers in the data and being less subjective to biasness in estimation of parameters [10,13,15,17]. Other studies have also been done using the regional L-moments approach for rainfall frequency analysis globally (e.g., United Kingdom [18], Italy [19], Norway [20]) and many regions of China (e.g., Guangxi [21], Yangtze River Delta region [22], Huaihe River Basin [23], Jiangxi [24,25], and Sichuan [26]). The research results indicated that this method is at an advantage on estimation of extreme quantiles over the at-site analysis under the conventional moments. In short, the regional L-moments method is able to solve the problems related to identification of homogeneous regions, testing and selection of the best fitting distributions, as well as estimations of parameters and quantiles at places of interest.

During 6–10 August 2009, Typhoon Morakot severely hit China's Taiwan Island and brought a large amount of rainfall with both high intensity and long duration to a wide area of the island, causing the worst flooding over southern Taiwan in the past 50 years. At Ali Mountain of Chiayi, the maximum 24- and 48-h accumulated rainfall reached 1623.5 mm and 2361.0 mm [27], respectively, which are close to the world records (i.e., 1825 mm for 24-h occurred on the Réunion Island in the Indian Ocean, and 2493 mm for 48-h occurred in Cherrapunji, Indian) [28]. Several important factors that contributed to the record-breaking rainfall have been analyzed in previous studies. One of them is the lifting effect of the mountainous topography of Taiwan, and the other is the persisting abundant moisture supply to southwestern Taiwan from the southwesterly moisture jet which leads to the substantially enhanced rainfall [29–33]. Therefore, if topographic influences can be removed from rainstorm of Typhoon Morakot through storm separation technique, the nontopographic rainfall component, or the convergence component, may be taken as a target transposition case for estimation of PMP in the east coast typhoon-prone areas of China [8,34,35].

In practice of PMP for Hong Kong, 4- and 24-h are two critical durations. Four-hour PMP is used for engineering design in terms of flood mitigation, and 24-h PMP can provide a reference for developing possible extreme event scenarios for designing landslide emergency preparedness measures [36]. Therefore, taking estimation of 4- and 24-h Hong Kong PMP for examples, this paper aims to propose an alternative sampling method for storm separation technique by replacing the annual maximum rainfalls by rainfall quantiles with rare probabilities via Regional L-moments Analysis (RLMA) for estimation of PMP.

The contents of this paper are structured as follows: Section 2 introduces the theoretical method of SDOIF and RLMA, alongside the procedure of PMP estimation using the proposed method. Following that, the study area and data sets used are described in Section 3. Subsequently, the results and discussion are given in Section 4, and the main conclusions are summarized in Section 5.

2. Methodology

2.1. Step-Duration-Orographic-Intensification-Factor (SDOIF) Method

For a rainstorm in mountainous areas, the rainfall intensity at a given point (place) (x, y) within a catchment at any time can be defined by:

$$I(x, y, t) = I_0(x, y, t) \times f(x, y, t) \quad (1)$$

where $I_0(x, y, t)$ is the convergence component and $f(x, y, t)$ is the orographic intensification factor (OIF) that presents the influence of weather system and topography respectively.

The average rainfall intensity during an interval of Δt is given below:

$$I_{\Delta t}(x, y) = I_{0,\Delta t}(x, y) \times f_{\Delta t}(x, y) \tag{2}$$

where $I_{0,\Delta t}(x, y)$ and $f_{\Delta t}(x, y)$ are the average values over Δt corresponding to the convergence component and the OIF respectively.

Thus, the rainfall amount $r_{\Delta t}(x, y)$ for a given point (place) in the time interval Δt can be obtained by:

$$r_{\Delta t}(x, y) = \int_{\Delta t} I(x, y, t)dt \approx I_{\Delta t}(x, y) \times \Delta t$$

$$= I_{0,\Delta t}(x, y) \times f_{\Delta t}(x, y) \times \Delta t = r_{0,\Delta t}(x, y) \times f_{\Delta t}(x, y) \tag{3}$$

where the $r_{0,\Delta t}(x, y)$ is the convergence rainfall without orographic influences for the given point (place) in Δt.

In practice, the average OIF of a point (place) (x, y) in the catchment of rainfall during the period Δt is written as:

$$OIF = \overline{f}_{\Delta t}(x, y) \approx \frac{\overline{R}_{\Delta t}(x, y)}{\overline{R}_{0,\Delta t}} \tag{4}$$

Considering PMP belongs to extreme events, the OIF $\overline{f}_{\Delta t}(x, y)$ for a particular duration is usually estimated based on annual maximum rainfall series of the corresponding duration. $\overline{R}_{\Delta t}(x, y)$ is the total rainfall containing the orographic influences measured by the average of annual maximum rainfalls for the corresponding duration. It is assumed that the rainfall on flatlands and/or the nearby coastal areas in the path of moisture inflow is not influenced by topography in terms of intensification. Therefore, stations located in these areas can be chosen as base stations to obtain the value of $\overline{R}_{0,\Delta t}$, the average convergence component. To reduce sampling error, the average of the means of annual maxima over selected base stations is used. Furthermore, this study attempts to use rainfall quantiles of different return periods instead of annual maxima for the calculation of OIF.

For a specific rainstorm, the convergence rainfall of a point (place) during the period Δt can be expressed as:

$$R_{0,\Delta t}(x, y) = \frac{R_{\Delta t}(x, y)}{OIF} = \frac{R_{\Delta t}(x, y)}{\overline{f}_{\Delta t}(x, y)} \tag{5}$$

where $R_{\Delta t}(x, y)$ is the observed maximum rainfall amount of the storm at the point and $\overline{f}_{\Delta t}(x, y)$ is the OIF from Equation (4).

2.2. Regional L-Moments Analysis (RLMA)

The general steps involved in the Regional L-moments Analysis (RLMA) using an index-flood procedure mainly include the following: identification of homogeneous regions, parameter estimation, choice of an appropriate probability distribution, estimation of quantiles, and internal consistency adjustment. The theory of RLMA and the methods used in these steps mentioned above are briefed in this section.

2.2.1. L-Moments Approach

L-moments are an alternative system to summarize the statistical properties of the hydrologic data and to describe the shape of the probability distributions. L-moments arose as modifications of the probability weighted moments (PWMs) of Greenwood et al. (1979) [37] and are defined by Hosking as expectations of certain linear combinations of order statistics [38]. Letting $X_{1:n} \leq X_{2:n} \leq \ldots \leq X_{n:n}$

be the order statistics of a random sample of size n drawn from the distribution of X, the L-moments of a probability distribution are defined by [10]:

$$\lambda_1 = E(X_{1:1})$$

$$\lambda_2 = \frac{1}{2}E(X_{2:2} - X_{1:2})$$

$$\lambda_3 = \frac{1}{3}E(X_{3:3} - 2X_{2:3} + X_{1:3})$$

$$\lambda_4 = \frac{1}{4}E(X_{4:4} - 3X_{3:4} + 3X_{2:4} - X_{1:4}) \quad (6)$$

and in general, the rth L-moment of variable X is:

$$\lambda_r = r^{-1}\sum_{k=0}^{r-1}(-1)^k \binom{r-1}{k} E(X_{r-k:r}),\ r = 1,\ 2,\ \ldots \quad (7)$$

where $E(X_{r-k:r})$ is the $(r-k)$th order statistics from a sample size of r.

Hosking defined the L-moment ratios as follows [10,38]:

$$\text{coefficient of L} - \text{variation}(L-Cv):\ \tau_2 = \lambda_2/\lambda_1$$

$$\text{coefficient of L} - \text{skewness}(L-Cs):\ \tau_3 = \lambda_3/\lambda_2$$

$$\text{coefficient of L} - \text{kurtosis}\ (L-Ck):\ \tau_4 = \lambda_4/\lambda_2 \quad (8)$$

2.2.2. The Index-Flood Procedure

The key assumption of an index-flood procedure is that the N sites form a homogeneous region and the frequency distributions of the N sites are identical apart from a site-specific scaling factor, the so-called index-flood which is a location estimator [10,12]. The location estimator is commonly the at-site sample mean $\overline{x}_i$. The frequency values q_{T_j} at several desired return periods T_j of the dimensionless regional distribution are called regional growth factors (RGFs). The quantiles for return periods T_j at site i can then be written as [12]:

$$Q_{T_j,i} = \overline{x}_i q_{T_j},\ j = 2\text{–},\ 5\text{–},\ \ldots,\ 100\text{–},\ \ldots,\ 1000 - year \quad (9)$$

The q_{T_j} can be determined by a set of regional parameters for a selected distribution. The regional parameters are weighted average values over N sites, with the parameter estimate of site i given weight proportional to the length of record, n_i. The at-site parameter estimate is obtained via the L-moments method based on rescaling data at site i to its mean $\overline{x}_i$.

2.2.3. Identification of Homogenous Regions

The aim of identifying homogenous regions is to form groups of sites that approximately satisfy the homogeneity condition. In the homogenous region, the statistical parameters ($L-Cv$, $L-Cs$, and $L-Ck$) of the sites are consistent within a tolerance. The measure to judge the degree of homogeneity of the region is [10]:

$$H_1 = \frac{V_{L-Cv} - \overline{V}_{L-Cv}}{\sigma_{L-Cv}} \quad (10)$$

where V_{L-Cv} is the variation of the $L-Cv$ over stations in a region. So, H_1 is the standardized V_{L-Cv}. Hosking suggested the region be regarded as "acceptably homogeneous" if $H_1 < 1$ [12]. The effect of $L-Cs$ on the formation of homogenous regions is also considered.

2.2.4. Selection of an Appropriate Probability Distribution

Three goodness-of-fit tests can be applied to select the best distribution in each region from five commonly used three-parameter frequency distributions: generalized logistic (GLO), generalized extreme-value (GEV), generalized normal (GNO), generalized Pareto (GPA), and Pearson type III (PE3).

Test 1: The Monte-Carlo simulation test.

The goodness-of-fit is judged by the deviation from the regional average of $L-Cs$ and $L-Ck$ of the observed data to the $L-Cs$ and $L-Ck$ of the fitted distribution. For each distribution, the measure is [10]:

$$Z^{DIST} = \left(\tau_4^{DIST} - t_4^R + \beta_4\right)/\sigma_4 \tag{11}$$

where "DIST" refers to the candidate distribution; t_4^R is the average $L-Ck$ value computed from the data of a given region; τ_4^{DIST} is the $L-Ck$ of the fitted distribution to the data using the candidate distribution; β_4 and σ_4 are the bias and standard deviation of the regional average $L-Ck$, t_4^R, of Monte-Carlo simulation samples by Kappa distribution.

For a confidence level of 90%, a distribution is acceptable if $\left|Z^{DIST}\right| \le 1.64$. Among accepted distributions, the distribution with the smallest $\left|Z^{DIST}\right|$ is the most appropriate $L-Ck$ distribution.

Test 2: Root Mean Square Error (RMSE) of the sample L-moments

RMSE is originated from the Four Criteria test [39]. In this test, a weighted RMSE calculated for each of the plausible distributions serves as an index. It is expressed by [13]:

$$RMSE = \left(\sum_{i=1}^{N} n_i\left(S_{i,L-Ck} - D_{i,L-Ck}\right)^2 / \sum_{i=1}^{N} n_i\right)^{\frac{1}{2}},\ i = 1,\ 2,\ \ldots,\ N \tag{12}$$

Here, n_i is the data length at site i; $S_{i,L-Ck}$ and $D_{i,L-Ck}$ are the sample $L-Ck$ and the distribution's $L-Ck$, respectively, at site i. The distribution with the smallest RMSE is the most appropriate distribution.

Test 3: Real-Data-Check (RDC) test

Having had a quantile estimate from a fitted distribution at a given return period T_j based on the real data series, an empirical exceedance frequency F_{i,T_j} to the quantiles can be calculated. Then F_{i,T_j} is compared with its corresponding theoretical probability P_{T_j}. A relative error (RE) can be calculated over several return periods to reflect the degree of the match between the empirical frequencies and the theoretical probabilities at site i. The smaller the RE is, the better the fitting will be. Then the regional averaged RE calculated over N sites in a homogeneous region can be used as an index for the goodness-of-fit [13]:

$$RE = \sum_{j}\sum_{i=1}^{N} \frac{\left(F_{i,T_j} - P_{T_j}\right)}{P_{T_j}} / \sum_{j}\sum_{i=1}^{N} 1,\ i = 1,\ 2,\ \ldots,\ N;\ j = 2-,\ 5-,\ \ldots,\ 100-year \tag{13}$$

For each return period, REs over the five three-parameter frequency distributions mentioned above are ranked from large to small, and the total ranking number over 2-, 5-, 10-, 25-, and 50-year for each distribution is taken as an index, called RE score, to evaluate the goodness of fit of the distribution. The higher the RE score is, the better the fitted distribution will be.

The above three goodness-of-fit tests are performed for each homogenous region and then a final decision to choose the most appropriate distribution can be made based on a summary of the tests' results.

2.3. Procedure of PMP Estimation

The flowchart of PMP estimation using the proposed storm separation technique is shown in Figure 1. For each rainfall duration, the following steps are taken:

(1) Estimation of rainfall quantiles via RLMA: Firstly, several homogeneous regions are identified in the target area based on historical annual maximum rainfalls, and the appropriate probability distributions for the regions are determined. Then, using the regional parameters of the identified distribution for each homogeneous region, quantile factors for the dimensionless distribution at specified recurrence intervals (or probabilities of nonexceedance) can be computed. By multiplying the quantile factors by the means of the at-site annual maximum rainfalls, the desired quantile estimates at sites are obtained.

(2) Development of OIF: Rainfall quantiles with certain return periods are used to calculate the OIFs at sites in the target area according to Equation (4). Then, a grid framework covering the target area is established at a resolution which is adapted to the spatial distribution density of raingauge stations. The Kriging method, which is an interpolation procedure used to estimate a variable at unsampled locations using weighted sums of the variable at neighboring sample points, is adopted to obtain the grid-point values of OIF.

(3) Storm Separation: The duration maximum rainfalls $R_{\Delta t}$ at sites are obtained based on observation data of the storms for transposition and then interpolated to the same grid framework of OIFs. At each grid point, using Equation (5) with $R_{\Delta t}$ as numerator and OIF as denominator, the convergence rainfall $R_{0,\Delta t}$ for each storm is achieved.

(4) Construction of the convergence component pattern: The spatial distribution of the convergence rainfall $R_{0,\Delta t}$ can be generalized into a set of concentric ellipses to build up the convergence component pattern. To determine the shape of the convergence component pattern, the most suitable ellipse for each convergence rainfall is drawn to fit the shape of isohyets around the rainfall center, and the aspect ratio (i.e., the ratio of the major radius to the minor radius) of each ellipse is estimated. The average of the aspect ratios over the storms is taken as the aspect ratio of the generalized convergence component pattern. Meanwhile, Depth-Area relation of each convergence rainfall is calculated. Taking the maximum area for every rainfall depth at an interval of 50mm in all storms, the Depth-Area relation of the generalized convergence component pattern is developed.

(5) Estimation of PMP: The convergence component pattern is transposed to the design area and coupled with (superposed onto) local OIFs. The OIFs of the design area is calculated in the same way as it is done for the target area. By multiplying the OIF by the rainfall value calculated from the isohyets of convergence component pattern at each grid point, the PMP estimates are achieved.

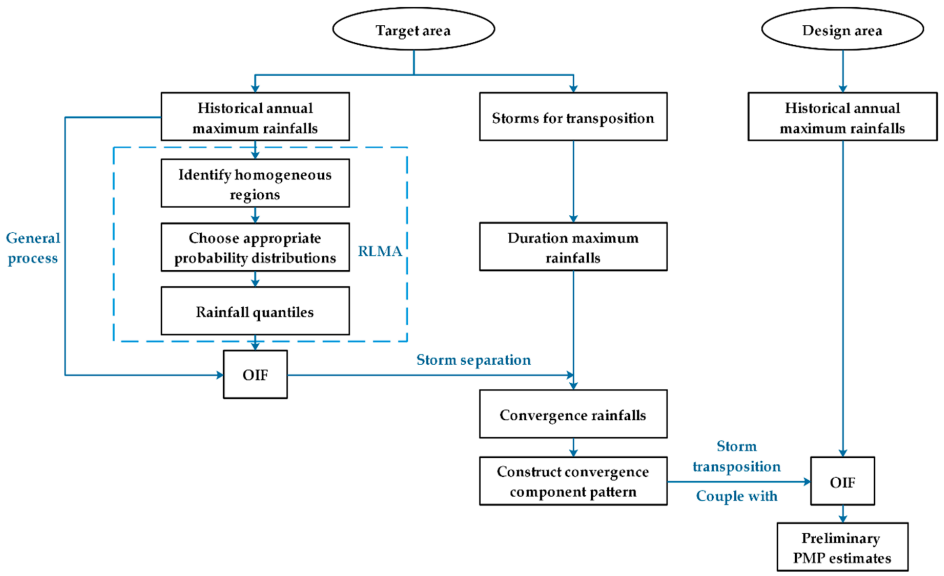

Figure 1. Flowchart of Probable Maximum Precipitation (PMP) estimation applying the storm separation technique using rainfall quantiles estimated via Regional L-moments Analysis (RLMA).

3. Study Area and Data Availability

The target area, Taiwan Island, lies off the southeast coast of mainland China with the geographic coordinates between 120° and 122° E longitude and 21.9° and 25.3° N latitude and covers a total area of about 35,800 km^2. As the elevation map shows (Figure 2a), two-thirds of the island are occupied by mountains which are mostly located in the central-east area of the island, while plains are mainly distributed in the west part. The five main mountain ranges, including Central, Jade, Snow, Ali, and Eastern Coastal Mountain Range, run approximately in parallel from north-northeast to south-southwest through the island, with a maximum elevation of 3952 m. The Central Mountain Range (CMR), which is high and steep, forms the backbone ridge. Many studies pointed out that when a typhoon passed over the island and its vicinity, enormous amounts of rainfall occurred and were enhanced by orographic lifting of the island mountains, particularly the CMR [40–43].

In this study, 4- and 24-h annual maximum rainfall series for the period of 1952–2019 at 181 raingauge stations in Taiwan were analyzed. As can be seen in Figure 2a, the selected stations are quite uniformly distributed in the plain area but are less dense in the mountain ranges. A preliminary quality control procedure for the data was carried out before it was used, such as removing obvious error records and evaluating the validity of the outliers. The average record length for these stations is 36 years with a range from 20 to 58 years. Besides, six outstanding severe storms in Taiwan all caused by tropical cyclones (TCs) with similarly southwesterly inflow of water vapor [32,44–47] have been selected for transposition analysis. Hourly precipitation observations from raingauge stations during the period of the TC were utilized to develop isohyets of duration rainfall maxima for each storm. The data periods and the duration rainfall maxima of selected storms are listed in Table 1. For 4-h, the transposed storm pattern is constructed based on storms of TCs Kalmaegi, Fanapi, Herb, and Morakot, the 4-h rainfall maxima of which are more than 400 mm. Storms of TCs Herb, Morakot, Haitang, and Aere were used for construction of the 24-h transposed storm pattern, the 24-h rainfall maxima of which are more than 1000 mm. Among them, 24-h rainfall maxima of Herb (1748.5 mm) is the maximum 24-h accumulated rainfall record in Taiwan [48]. Considering the moisture inflow direction of the storms, five stations (i.e., Puzi, Beimen, Xiaying, Yongkang, Kaohsiung), which are located in the southwestern coastal plain of Taiwan Island with the elevation lower than 20 m (red squares in Figure 2a), were selected as the base stations for the development of OIF.

The design area of PMP is Hong Kong, which lies in the south of China and has an area of about 1104 km^2. To develop the local OIF, historical 4- and 24-h annual maximum rainfall data of 73 raingauge stations in Hong Kong and Shenzhen station in Guangdong province of China located close to Hong Kong (Figure 2b) with observation periods longer than 20 years have been used. The main inflow direction of moisture during typhoon storms in Hong Kong is northeast or north [34,35], so R22, R30, and Shenzhen, located in the northern low-altitude area (red squares in Figure 2b), were selected as the base stations.

Table 1. Data periods and duration rainfall maxima of selected storms (listed with corresponding tropical cyclones—TCs) for 4- and 24-h transposition analysis.

TCs	Storm Data Period	4-h Rainfall Maxima (mm)	24-h Rainfall Maxima (mm)
Kalmaegi (2008)	16–18 July	496.0	-
Fanapi (2010)	17–20 September	435.5	-
Herb (1996)	29 July–1 August	415.5	1748.5
Morakot (2009)	5–10 August	404.5	1623.5
Haitang (2005)	16–20 July	-	1254.5
Aere (2004)	24–26 August	-	1154.0

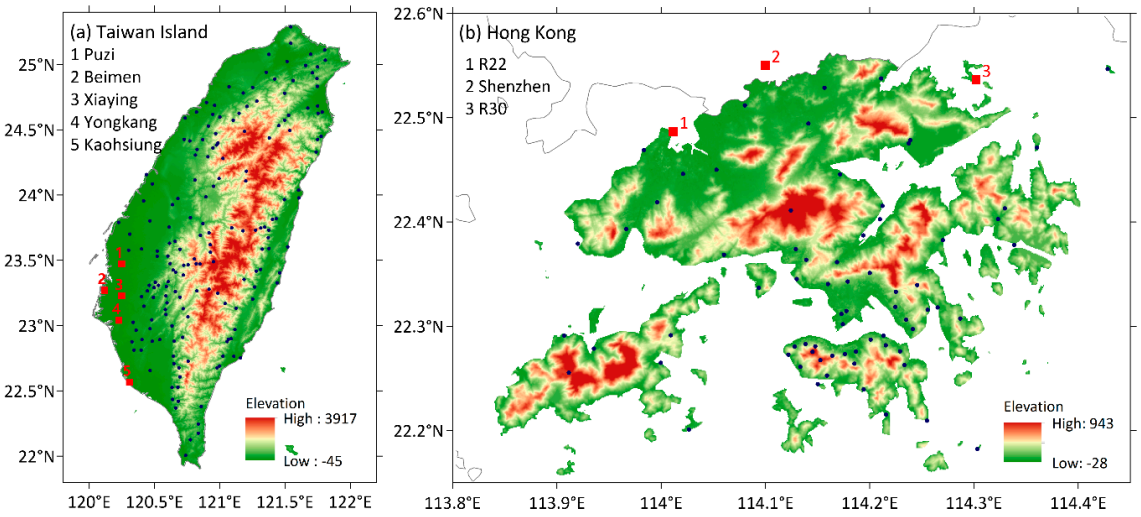

Figure 2. Elevation map of (**a**) Taiwan Island and (**b**) Hong Kong, and locations of the raingauge stations. Red squares indicate selected base stations for development of orographic intensification factor (OIF).

4. Results and Discussion

4.1. Homogeneous Regions of Taiwan

According to the criteria for identifying homogenous regions mentioned above, Taiwan area was preliminarily delineated into eight subregions for 4- and 24-h, respectively (Figure 3). Tables 2 and 3 present the homogeneity measure H_1 and the goodness-of-fit tests' results of each subregion for 4- and 24-h. All the values of H_1 are less than 1, meaning that the grouping is reasonable in term of homogeneity. In each test, the distributions ranked first or second in performance of the fit may be considered as the appropriate ones. Then taking into consideration of all the three goodness-of-fit tests' results, the best-fit distributions for the homogeneous regions are determined, respectively. For 4-h, GEV distribution fits best for most of the homogeneous regions, expect for region 3 and 4 for which GNO distribution is the best one. While for 24-h, GNO distribution is best fitted for half of the homogeneous regions.

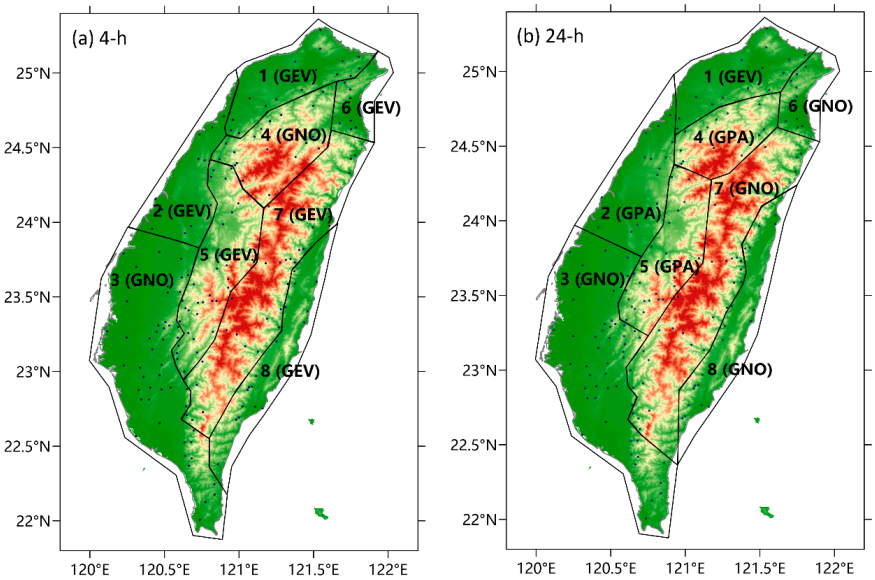

Figure 3. Sketch of (**a**) 4-h and (**b**) 24-h homogeneous regions of Taiwan and the best-fit distributions for homogeneous regions.

Table 2. Numbers of sites, values of homogeneity measure H_1, and goodness-of-fit tests' results, as well as the best-fit distributions for 4-h homogenous regions of Taiwan (The best fitting results of each test are highlighted in bold, and '-' indicates the value of $|Z^{DIST}|$ exceeds 1.64.).

Homogenous Regions	Number of Sites	H_1	Z^{DIST}					RMSE(E−5)					RE Score					Best-Fit Distribution
			GLO	GEV	GNO	GPA	PE3	GLO	GEV	GNO	GPA	PE3	GLO	GEV	GNO	GPA	PE3	
1	17	0.79	1.38	**−0.66**	−1.16	-	-	6186	**4880**	5139	9886	6192	**17.0**	**17.0**	**17.0**	9.0	15.0	**GEV**
2	11	−1.09	1.28	**0.05**	−0.57	-	-	7515	**5153**	5221	6948	6767	12.5	16.5	**17.0**	14.0	15.0	**GEV**
3	49	0.75	-	**0.15**	−0.58	-	-	7216	5465	**5346**	9567	5718	10.0	15.5	**20.5**	10.0	19.0	**GNO**
4	19	0.85	-	-	1.38	-	**0.21**	9171	6113	**6016**	6712	6109	13.0	**18.0**	**18.0**	11.0	15.0	**GNO**
5	33	0.44	-	0.97	**0.08**	-	−1.63	9110	**6817**	6873	8386	7563	11.0	**18.5**	16.5	11.0	18.0	GEV
6	7	0.13	1.61	**0.10**	−0.25	-	−0.98	6077	**2391**	2970	7408	4273	12.0	18.0	**18.5**	11.0	15.5	**GEV**
7	28	0.23	-	**−1.18**	−1.37	-	-	6731	**5660**	5905	11331	6718	**18.5**	**18.5**	17.5	5.0	15.5	**GEV**
8	17	−0.2	**0.60**	−1.57	-	-	-	6532	**6373**	6424	12,337	7073	14.5	**18.0**	16.5	9.0	17.0	**GEV**

Table 3. Numbers of sites, values of homogeneity measure H_1 and goodness-of-fit tests' results, as well as the best-fit distributions for 24-h homogenous regions of Taiwan (The best fitting results of each test are highlighted in bold, and '-' indicates the value of $|Z^{DIST}|$ exceeds 1.64.).

Homogenous Regions	Number of Sites	H_1	Z^{DIST}					RMSE(E−5)					RE Score					Best-fit Distribution
			GLO	GEV	GNO	GPA	PE3	GLO	GEV	GNO	GPA	PE3	GLO	GEV	GNO	GPA	PE3	
1	15	−1.74	1.15	**−0.42**	−1.05	-	-	6982	**5754**	6226	9678	7745	16.0	**17.5**	16.5	11.0	14.0	**GEV**
2	15	−0.89	-	-	-	**−0.76**	1.57	13,280	10,534	9837	**6889**	9068	7.0	12.0	14.0	**22.0**	20.0	**GPA**
3	51	0.45	-	-	**0.80**	-	−1.15	9490	7420	**7221**	9114	7407	13.5	19.0	**20.0**	8.5	14.0	**GNO**
4	14	−0.89	-	-	-	**−1.35**	-	12,353	9400	8983	**6463**	8532	11.0	13.5	16.5	**17.5**	16.5	**GPA**
5	26	0.51	-	-	-	**−0.53**	-	12,462	9376	8609	**5716**	7323	9.5	12.5	16.5	16.5	**20.0**	**GPA**
6	9	−0.56	-	0.38	**−0.18**	-	−1.22	6296	3630	**3595**	7297	4542	13.0	**15.5**	**15.5**	**15.5**	**15.5**	**GNO**
7	31	0.58	-	0.11	**0.08**	-	−0.71	8553	**5841**	6323	9561	6641	12.5	14.5	**18.0**	13.0	17.0	**GNO**
8	20	0.93	-	−0.64	**0.00**	-	−0.16	8259	**6323**	6953	12,169	7601	17.5	15.5	**18.5**	5.0	**18.5**	**GNO**

4.2. Rainfall Quantiles in Taiwan

The rainfall quantiles at recurrence intervals of 100, 200, and 500 years at sites in Taiwan were obtained for the subsequent processing. Internal consistency check of 100-, 200-, and 500-year quantiles over 4- and 24-h was also performed for each site. Results show that there is no situation that the quantile of 4-h is larger than that of 24-h at one site. Table 4 gives 4- and 24-h means of annual maximum rainfalls and rainfall quantiles of selected base stations and top-ranked-rainfall stations. It shows that, no matter what values of the means of annual maxima or quantiles, they are much smaller in magnitude at base stations than at those stations with top-ranked rainfall maxima. This is because the base stations are located at much lower elevation near coastal area and considered not influenced by topography in terms of intensification. It clearly indicates that the topography does have impact on rainfall in mountainous areas over a long period of time.

Table 4. Four and 24-h means of annual maximum rainfalls along with 100-, 200-, and 500-year rainfall quantiles of selected base stations (station 1–5) and top-ranked-rainfall stations (station 6–9).

	Station	Longitude (° E)	Latitude (° N)	4-h (mm)				24-h (mm)			
				Means of Annual Maxima	Quantiles			Means of Annual Maxima	Quantiles		
					100-year	200-year	500-year		100-year	200-year	500-year
1	Puzi	120.25	23.47	114.8	252.3	277.1	310.5	239.9	623.1	695.2	793.3
2	Beimen	120.12	23.27	101.6	223.4	245.3	274.9	224.8	583.8	651.3	743.3
3	Xiaying	120.25	23.23	119.8	263.3	289.2	324.0	267.2	693.8	774.1	883.3
4	Yongkang	120.23	23.04	122.9	270.3	296.8	332.6	281.1	730.1	814.6	929.5
5	Kaohsiung	120.31	22.57	129.7	285.1	313.1	350.8	280.6	728.8	813.0	927.8
6	Xinmajia	120.69	22.68	231.3	510.4	555.2	613.0	673.8	1630.8	1781.8	1979.4
7	Taiwu	120.70	22.61	226.8	498.8	547.8	613.7	656.6	1589.3	1736.4	1929.0
8	Ali	120.76	22.73	196.4	433.4	471.5	520.5	581.3	1406.9	1537.2	1707.6
9	Alishan	120.81	23.51	182.2	478.3	540.6	628.3	578.7	1536.9	1625.0	1716.9

4.3. Orographic Intensification Factor (OIF) of Taiwan under Southwesterly Moisture Inflow

In this study, four data samples (i.e., annual maximum rainfalls, 100-, 200-, and 500-year rainfall quantiles) were used to develop OIF in Taiwan for comparison. Given the spatial distribution density of raingauge stations (i.e., one station per 200 km^2), the OIFs at sites were interpolated to the gird with a resolution of 14 km × 14 km (0.125° × 0.125°). The spatial distributions of OIFs based on annual maximum rainfalls, 100-, 200-, and 500-year rainfall quantiles (hereafter, OIF_{am}, $OIF_{100\text{-}yr}$, $OIF_{200\text{-}yr}$, and $OIF_{500\text{-}yr}$, respectively) are shown in Figure 4. It can be observed that, for the same duration, the spatial distribution patterns of OIF_{am}, $OIF_{100\text{-}yr}$, $OIF_{200\text{-}yr}$, and $OIF_{500\text{-}yr}$ are similar, which illustrates that OIFs can stably reflect the influences of topography on precipitation. The areas of high OIF values are mainly in the southwestern of Ali, Jade, and Central Mountain Range, with the two highest value centers located around Ali Mountain (denoted by C1) and Weiliao Mountain (denoted by C2) and in the windward slope of the mountains with obvious topographic lifting effect under the southwesterly moisture inflow during typhoon storms. The two maximum total accumulated rainfall records during Typhoon Morakot from 5 to 10 August 2009 were observed in Ali Mountain (3059.5 mm) and Weiliao Mountain (2910.0 mm), which are consistent with these two OIF centers. Comparing to 4-h OIFs, the center values of 24-h OIFs are larger, and the contours of 24-h OIFs are denser, which indicates that the influences of topography on rainfall enhances with the increase of duration. In addition, it is found that there is another high value center of 24-h OIFs in the northeast of Taiwan, where high rainfall records were also observed in history. However, given that the OIFs were developed under southwesterly moisture inflow while the northeastern area is in the leeward side of the mountain ranges with respect to the southwesterly moisture inflow, it is not considered in question.

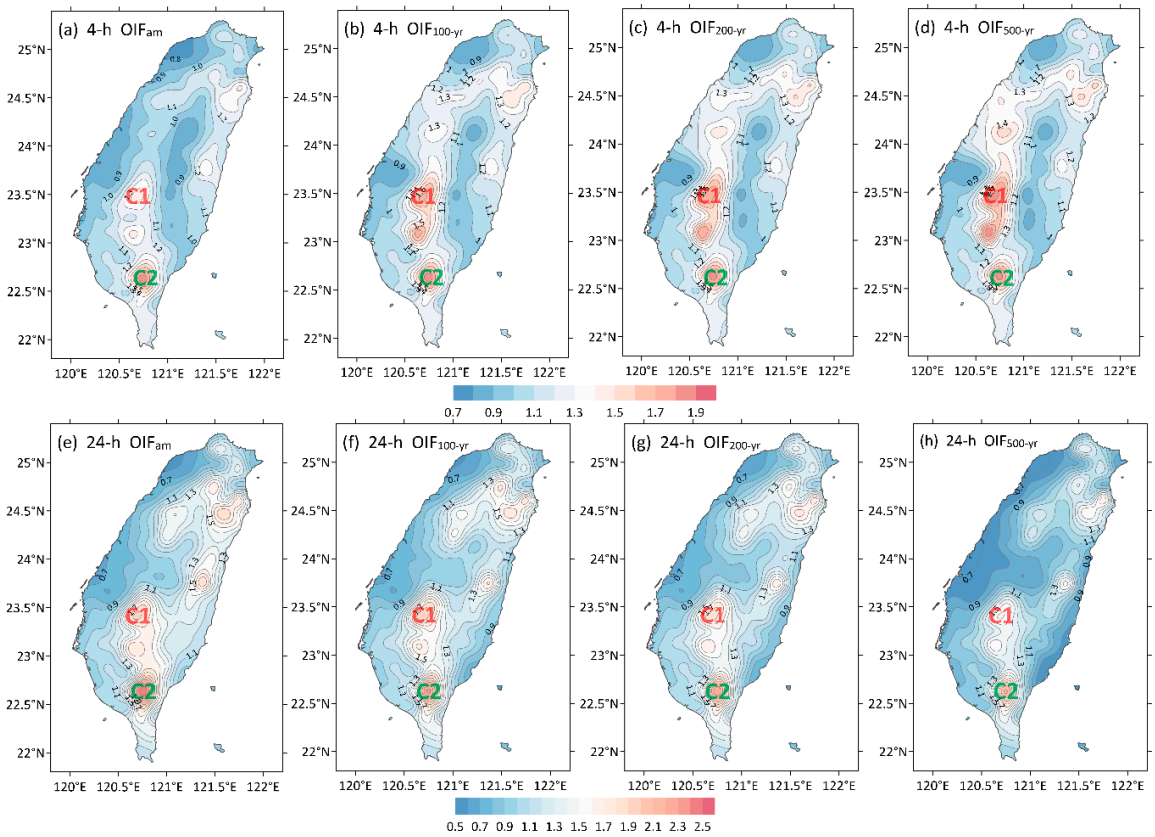

Figure 4. Spatial distribution maps of Taiwan (**a**–**d**) 4-h and (**e**–**h**) 24-h OIFs under southwesterly moisture inflow: (**a**,**e**) based on annual maximum rainfalls (OIF_{am}); (**a**,**f**) based on 100-year rainfall quantiles ($OIF_{100\text{-}yr}$); (**b**,**g**) based on 200-year rainfall quantiles ($OIF_{200\text{-}yr}$); (**c**,**h**) based on 500-year rainfall quantiles ($OIF_{500\text{-}yr}$). C1 and C2 indicate the high value centers of OIFs at Ali and Weiliao Mountain, respectively.

As presented in Figure 4, the isohyets of $OIF_{100\text{-}yr}$, $OIF_{200\text{-}yr}$, and $OIF_{500\text{-}yr}$ are denser and telling more spatial details than that of OIF_{am}. Figure 5 gives the differences between the OIFs based on rainfall quantiles and OIF_{am}. It is observed that, to the west windward slopes of the Central Mountain Range (CMR), as well as at the high value center around Ali Mountain, where the orographic effect is strong, 4-h $OIF_{100\text{-}yr}$, $OIF_{200\text{-}yr}$, and $OIF_{500\text{-}yr}$ are slightly higher than OIF_{am} but slightly lower than OIF_{am} to the east of CMR. Moreover, OIF_{am}, $OIF_{100\text{-}yr}$, $OIF_{200\text{-}yr}$, and $OIF_{500\text{-}yr}$ are close to each other on the southwestern coastal plain. While for a longer duration of 24-h, $OIF_{200\text{-}yr}$, and $OIF_{500\text{-}yr}$ are close to OIF_{am} to the west and south of Taiwan, and just the $OIF_{100\text{-}yr}$, which reflects the orographic effect more evidently, are higher than OIF_{am} around Ali Mountain. This may suggest that the 100-year quantiles based on current data situation are more stable and hence of more representativeness to the Ali Mountain in terms of the rainfall intensification.

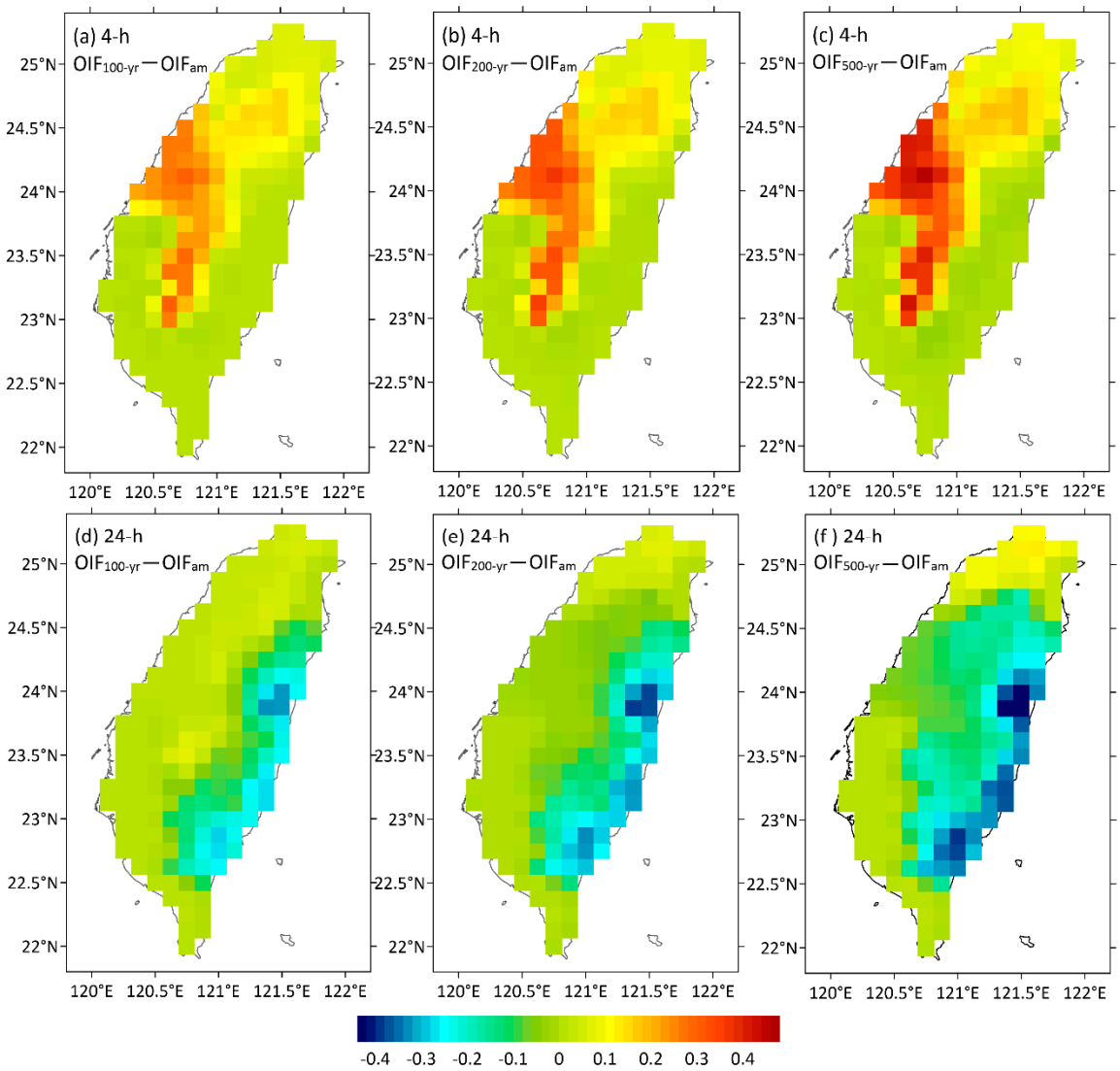

Figure 5. Differences of (**a**–**c**) 4-h and (**d**–**f**) 24-h OIFs based on annual maximum rainfalls, 100-, 200-, and 500-year rainfall quantiles: (**a**,**d**) $OIF_{100\text{-yr}}$—OIF_{am}; (**b**,**e**) $OIF_{200\text{-yr}}$—OIF_{am}; (**c**,**f**) $OIF_{500\text{-yr}}$—OIF_{am}.

4.4. Storm Separation and Construction of the Convergence Component Pattern

For each duration, the selected four storms were separated by OIF_{am}, $OIF_{100\text{-yr}}$, $OIF_{200\text{-yr}}$, and $OIF_{500\text{-yr}}$ separately in a 0.125° (14 km) latitude–longitude resolution grid (same as the grid framework for interpolated OIFs). Then convergence rainfalls of the four storms based on annual maximum rainfalls, 100-, 200-, and 500-year rainfall quantiles (hereafter, $R_{0(am)}$, $R_{0(100\text{-yr})}$, $R_{0(200\text{-yr})}$, and $R_{0(500\text{-yr})}$, respectively) were obtained. The center values of rainfalls before and after separation are given in Table 5. The first row gives the 4- and 24-h maximum observed rainfalls ($R_{\Delta t}$) which contain the orographic effects. It is obvious that, after removing the orographic effects, the maximum convergence rainfalls ($R_{0(am)}$, $R_{0(100\text{-yr})}$, $R_{0(200\text{-yr})}$, and $R_{0(500\text{-yr})}$) are smaller than maximum $R_{\Delta t}$ of the corresponding storms. The differences between the observed rainfalls and the convergence rainfalls are larger for longer duration than that for shorter duration, which indicates that the orographic effects are stronger for longer duration. The 4-h maximum $R_{0(100\text{-yr})}$, $R_{0(200\text{-yr})}$, and $R_{0(500\text{-yr})}$ are generally close and slightly smaller than maximum $R_{0(am)}$. However, the 24-h maximum $R_{0(100\text{-yr})}$, $R_{0(200\text{-yr})}$, and $R_{0(500\text{-yr})}$ are much larger than maximum $R_{0(am)}$ and increase with the increasing return periods. All these indicate that the orographic impacts on rainfall increase with increase of duration of rainfall.

Table 5. Center values of the observed rainfalls ($R_{\Delta t}$) and the convergence rainfalls ($R_{0(am)}$, $R_{0(am)}$, $R_{0(200\text{-}yr)}$, and $R_{0(500\text{-}yr)}$) for 4- and 24-h.

Rainfall Category	4-h (mm)				24-h (mm)			
	Kalmaegi	Fanapi	Herb	Morakot	Herb	Morakot	Haitang	Aere
$R_{\Delta t}$	496.00	435.50	415.50	404.50	1748.50	1623.50	1254.50	1154.00
$R_{0(am)}$	326.74	295.15	256.90	309.35	717.01	842.78	541.89	683.00
$R_{0(100\text{-}yr)}$	306.14	295.39	214.66	283.11	700.13	883.40	586.64	670.02
$R_{0(200\text{-}yr)}$	302.68	295.40	208.46	280.19	739.50	901.67	599.61	707.82
$R_{0(500\text{-}yr)}$	298.26	295.41	200.88	276.76	799.96	940.27	616.61	765.55

The spatial distribution of 4- and 24-h convergence rainfalls are shown in Figures 6 and 7. For the same duration and the same storm, the spatial distribution patterns of convergence rainfalls based on different data samples are similar, so the shapes of the isohyets around the rainfall centers could be fitted by the same generalized ellipse (red ellipses in Figures 6 and 7). Then the aspect ratio of the generalized convergence component pattern for each duration was obtained by averaging the aspect ratios of the four generalized ellipses. They are 1.5375 and 1.5125 for 4- and 24-h, respectively, which are very close. The Depth-Area relation of 4- and 24-h generalized convergence component patterns based on different data samples are given in Tables 6 and 7. For 4-h convergence component patterns, the pattern of $R_{0(am)}$ has the highest center value and the largest areas in every rainfall depth interval. However, it shows an opposite situation for 24-h.

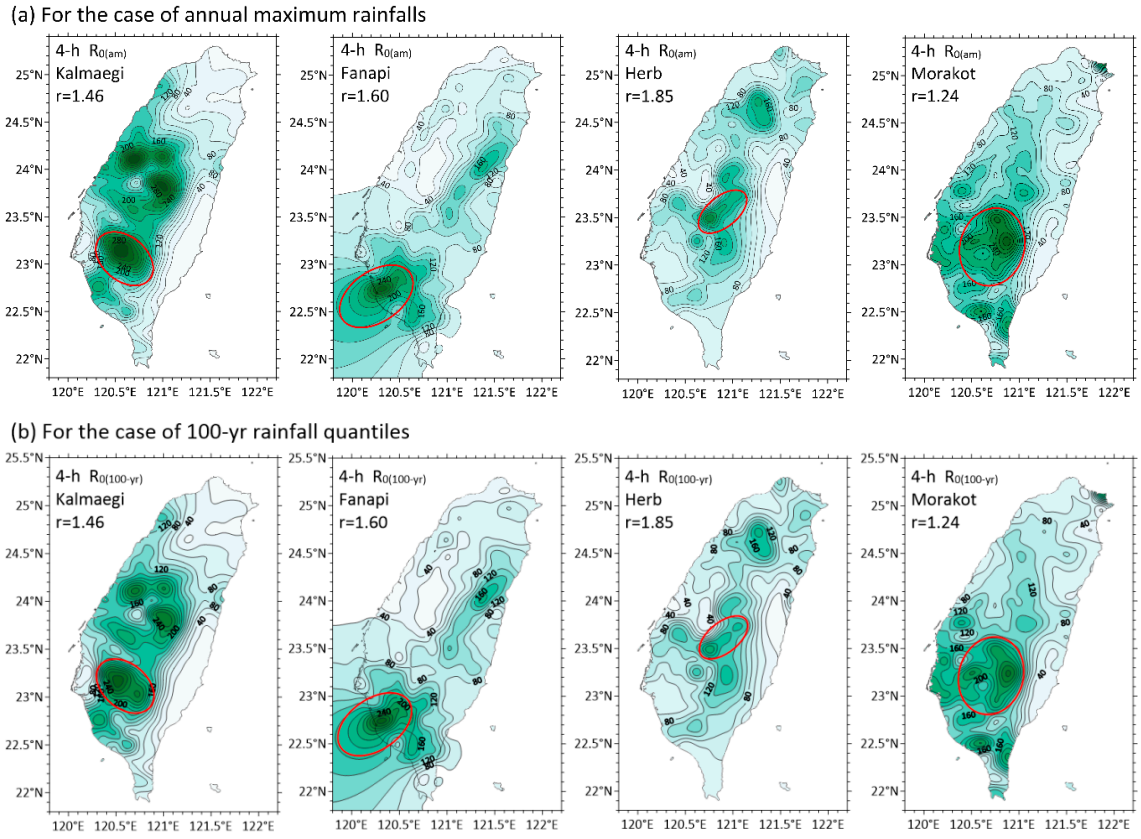

Figure 6. *Cont.*

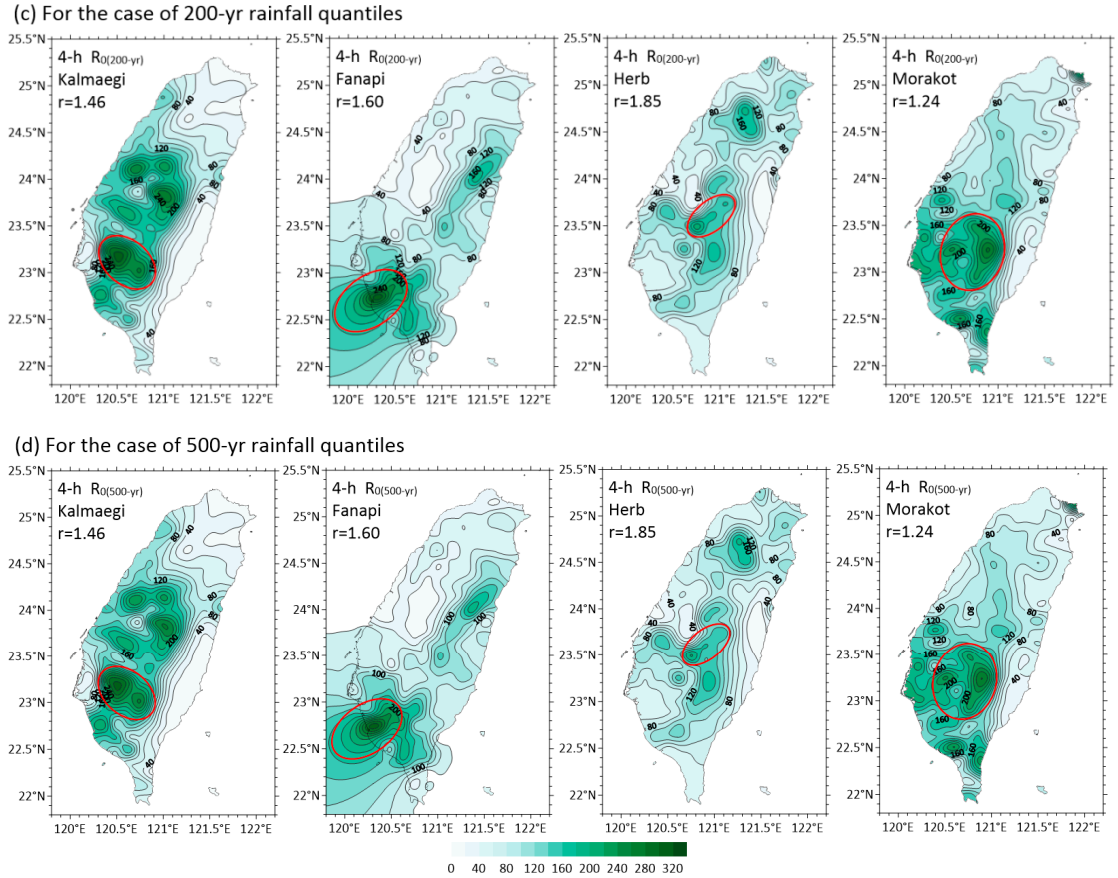

Figure 6. Four-hour convergence rainfall isohyetal maps of storms of TCs Kalmaegi, Fanapi, Herb, and Morakot affecting Taiwan for the cases of (**a**) annual maximum rainfalls, (**b**) 100-year rainfall quantiles, (**c**) 200-year rainfall quantiles, and (**d**) 500-year rainfall quantiles. Red circles and r denote the generalized ellipses for the convergence rainfalls and their aspect ratios, respectively.

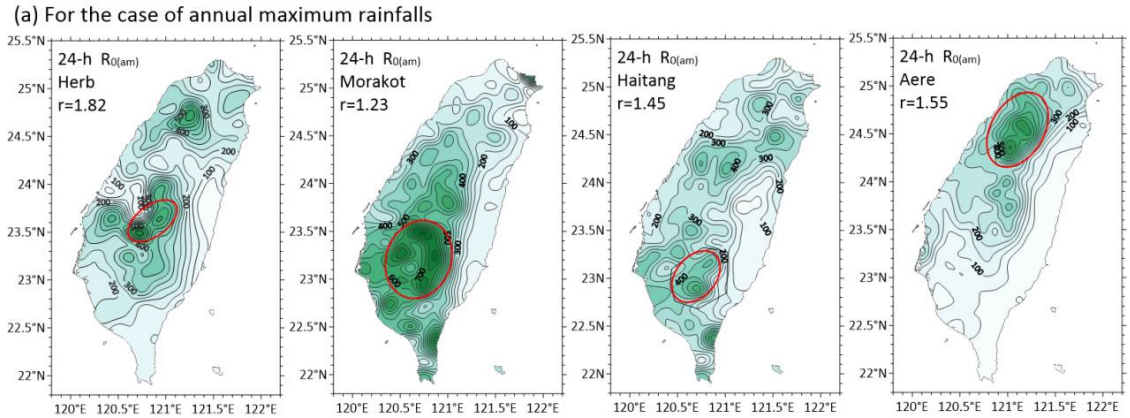

Figure 7. *Cont.*

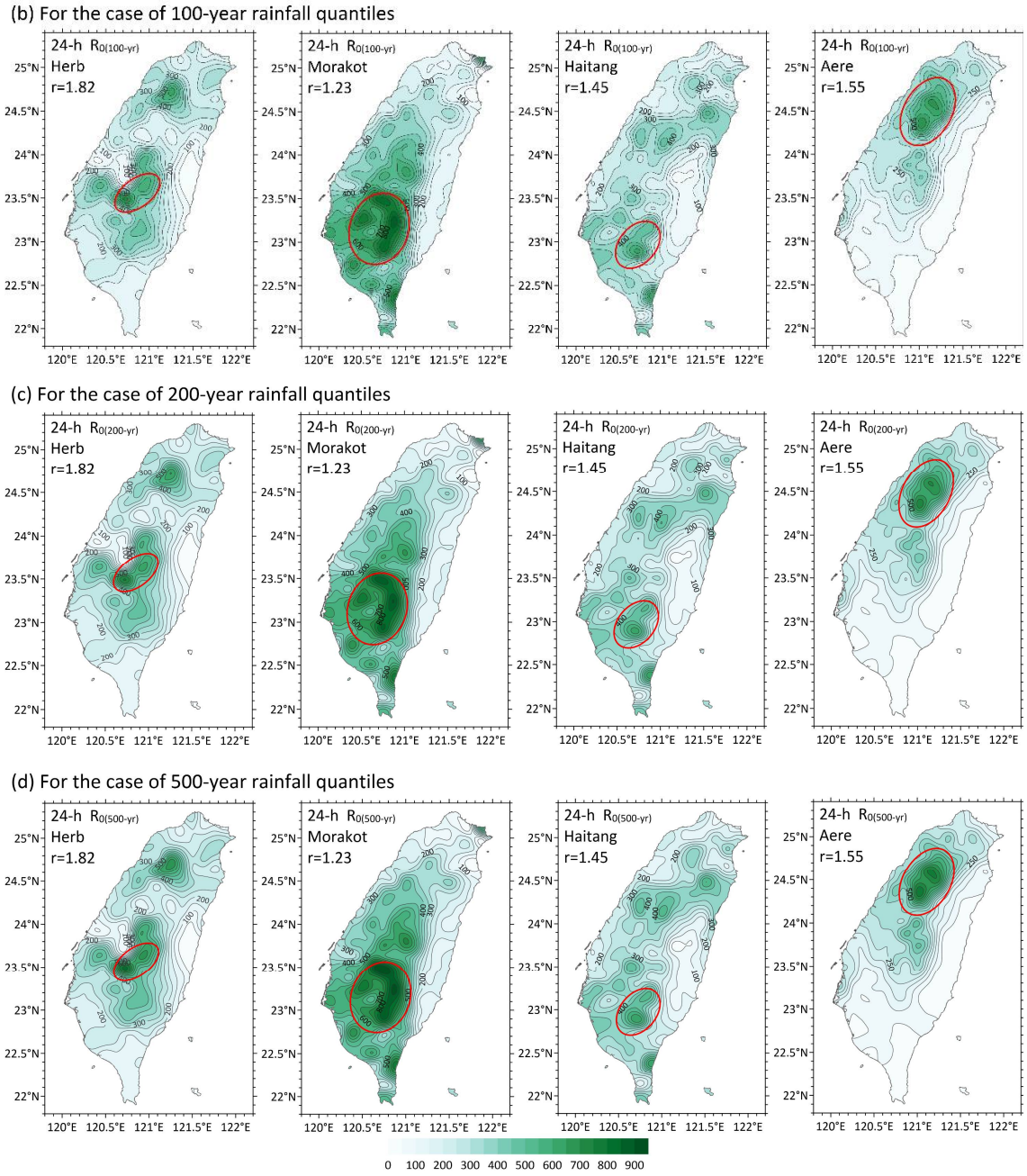

Figure 7. Twenty-four-hour convergence rainfall isohyetal maps of storms of TCs Herb, Morakot, Haitang, and Aere affecting Taiwan for the cases of (**a**) annual maximum rainfalls, (**b**) 100-year rainfall quantiles, (**c**) 200-year rainfall quantiles, and (**d**) 500-year rainfall quantiles. Red circles and r denote the generalized ellipses for the convergence rainfalls and their aspect ratios, respectively.

Table 6. Depth-Area relation of 4-h convergence component patterns based on annual maximum rainfalls, 100-, 200-, and 500-year rainfall quantiles.

Isohyets (mm)	Area (km^2)			
	Pattern of $R_{0(am)}$	Pattern of $R_{0(100\text{-}yr)}$	Pattern of $R_{0(200\text{-}yr)}$	Pattern of $R_{0(500\text{-}yr)}$
50	31,881.70	31,447.68	31,373.12	31,266.79
100	20,816.35	18,378.25	18,094.28	17,761.58
150	12,231.82	10,470.06	10,014.78	9605.52
200	3119.37	2237.58	2102.96	1984.52
250	1207.39	903.03	790.83	701.39
300	453.42	124.38	97.51	-

Table 7. Depth-Area relation of 24-h convergence component patterns based on annual maximum rainfalls, 100-, 200-, and 500-year rainfall quantiles.

Isohyets (mm)	Area (km^2)			
	Pattern of $R_{0(am)}$	Pattern of $R_{0(100\text{-}yr)}$	Pattern of $R_{0(200\text{-}yr)}$	Pattern of $R_{0(500\text{-}yr)}$
50	35,245.02	35,325.08	35,349.79	35,385.68
100	33,650.13	34,347.81	34,232.98	34,062.31
150	29,288.53	29,923.18	30,044.69	30,518.39
200	25,872.61	26,161.95	26,377.82	26,666.98
250	23,209.88	23,518.93	23,866.45	24,289.69
300	19,818.52	20,117.71	20,891.05	21,809.99
350	17,690.70	18,103.19	18,471.69	19,131.15
400	14,596.24	15,016.58	15,973.14	16,972.45
450	11,985.35	12,410.95	12,933.63	13,889.52
500	8661.74	8747.52	9278.78	10,006.27
550	6598.92	6668.70	7222.13	7950.74
600	3946.10	4204.51	4337.09	4511.36
650	2748.03	3064.23	3338.07	3569.35
700	1758.12	2059.28	2322.65	2704.62
750	912.99	1357.74	1614.58	1951.11
800	250.40	639.10	988.28	1351.21
850	-	96.63	305.79	811.66
900	-	-	7.69	236.72

4.5. PMP Estimates in Hong Kong

For the sake of comparison, only 4- and 24-h OIF_{am} of Hong Kong based on annual maximum rainfalls was used. The resolution of the compute grid is 0.05° × 0.05° (5 km × 5 km) which is adapted to the spatial distribution density of raingauge stations in Hong Kong. The gridded values of OIF_{am} are presented in Figure 8. It can be seen both the maximum 4- and 24-h OIF_{am} of Hong Kong are centered at 114.15° E, 22.4° N near Tai Mo Mountain (marked in red star), at which the centers of convergence component patterns (red ellipses in Figure 8) were placed. Then the preliminary PMP estimates for generalized $R_{0(am)}$, $R_{0(100\text{-}yr)}$, $R_{0(200\text{-}yr)}$, and $R_{0(500\text{-}yr)}$ (hereafter, PMP_{am}, $PMP_{100\text{-}yr}$, $PMP_{200\text{-}yr}$, and $PMP_{500\text{-}yr}$, respectively) were obtained on the grid, and the isohyets of the PMP were drawn up (Figure 9). The superposition of the generalized convergence component patterns transposed from Taiwan onto the local orographic component was made at orientations of several directions. For simplicity, the results at east–west orientation shown here are for illustration.

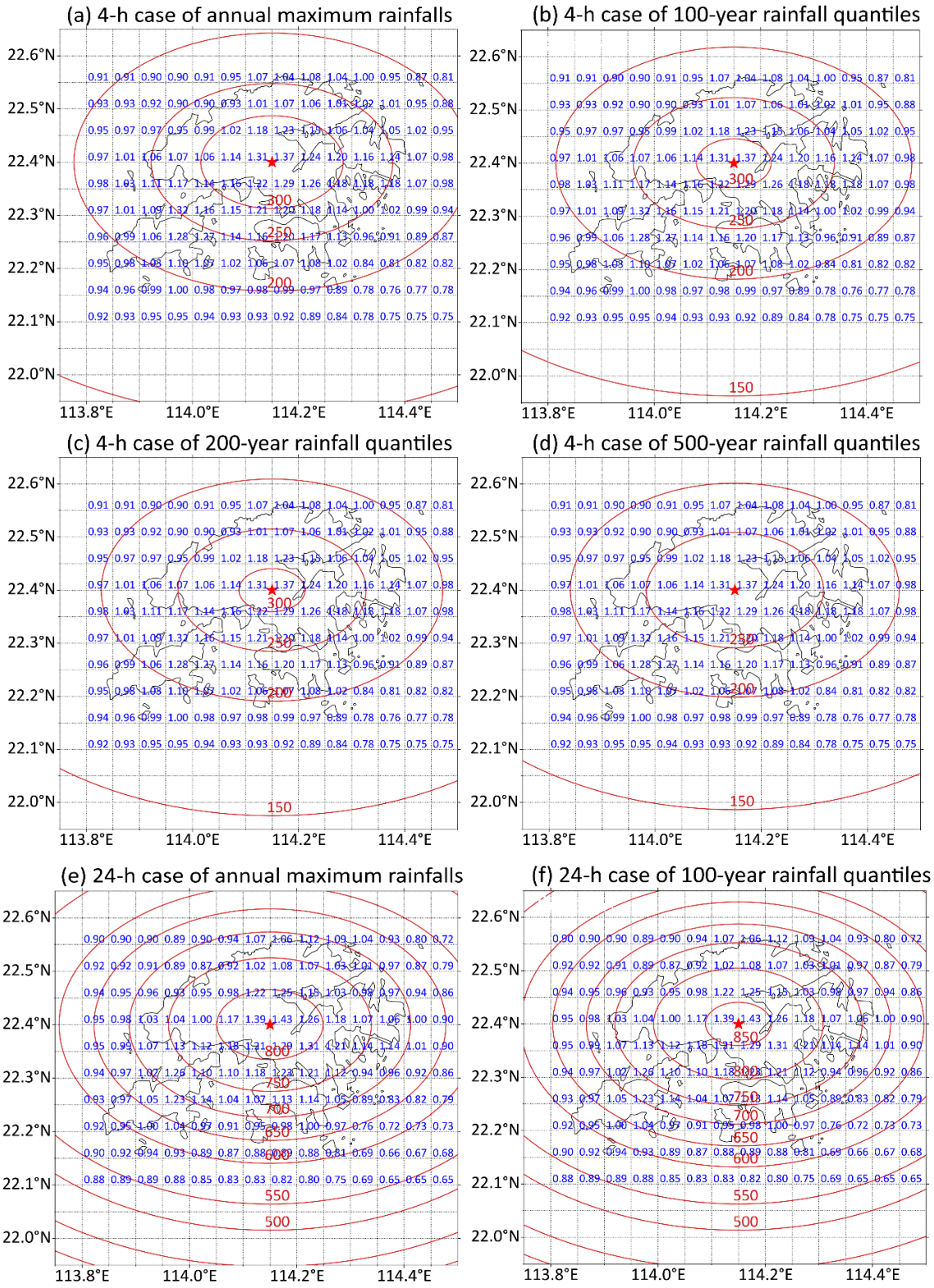

Figure 8. *Cont.*

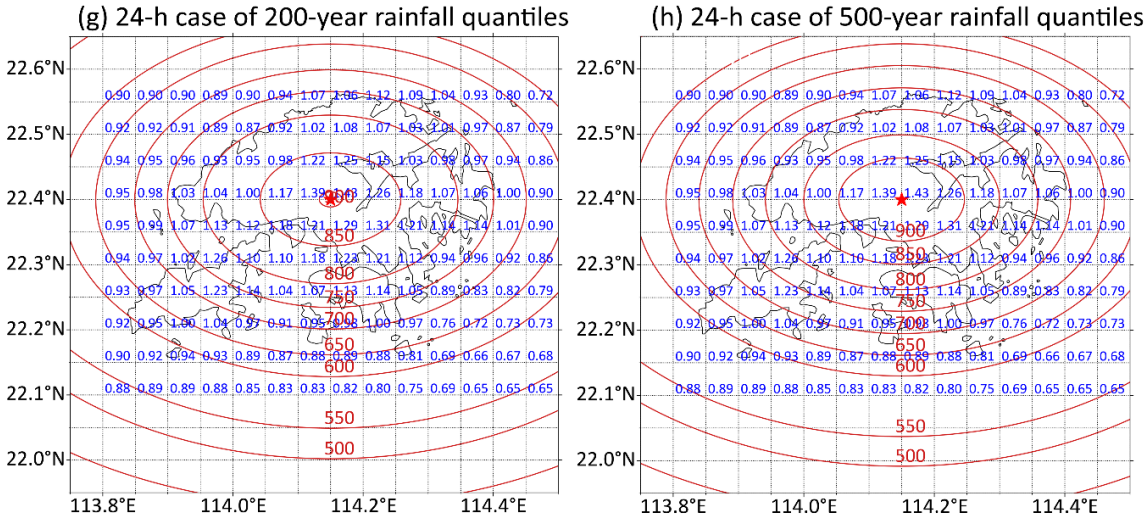

Figure 8. (**a**–**d**) 4-h and (**e**–**h**) 24-h generalized convergence component patterns of Taiwan storms (red ellipses) superposed on Hong Kong gridded OIFs (blue numbers, grid resolution: 5 km × 5 km) for the cases of (**a**,**e**) annual maximum rainfalls, (**b**,**f**) 100-year rainfall quantiles, (**c**,**g**) 200-year rainfall quantiles, and (**d**,**h**) 500-year rainfall quantiles.

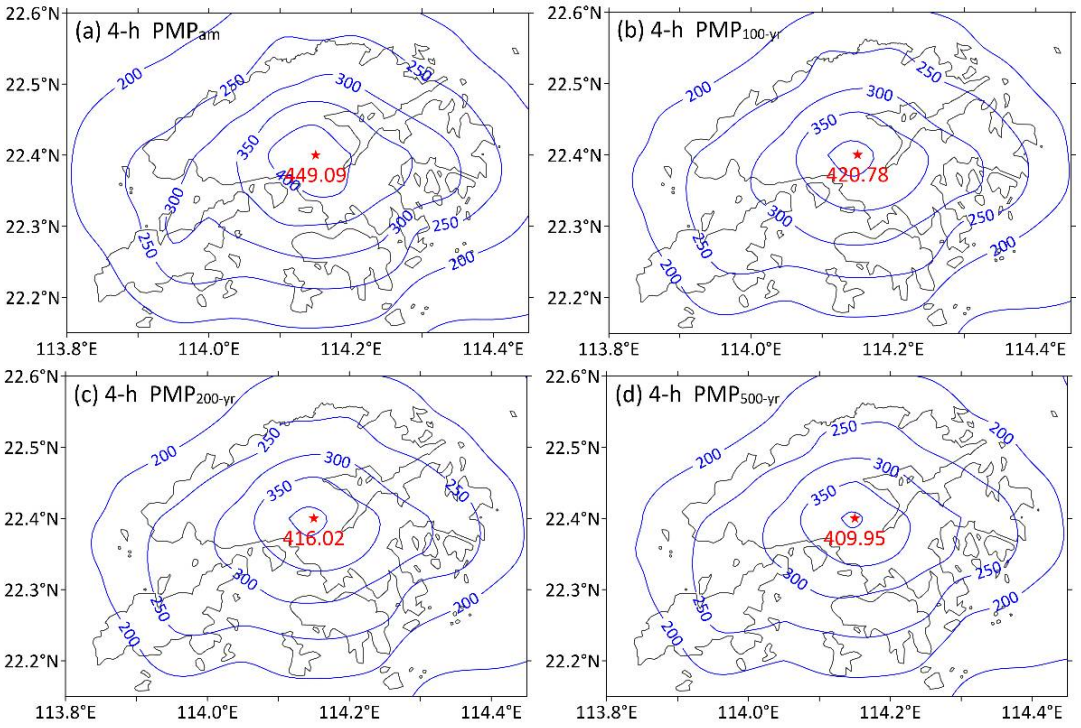

Figure 9. *Cont.*

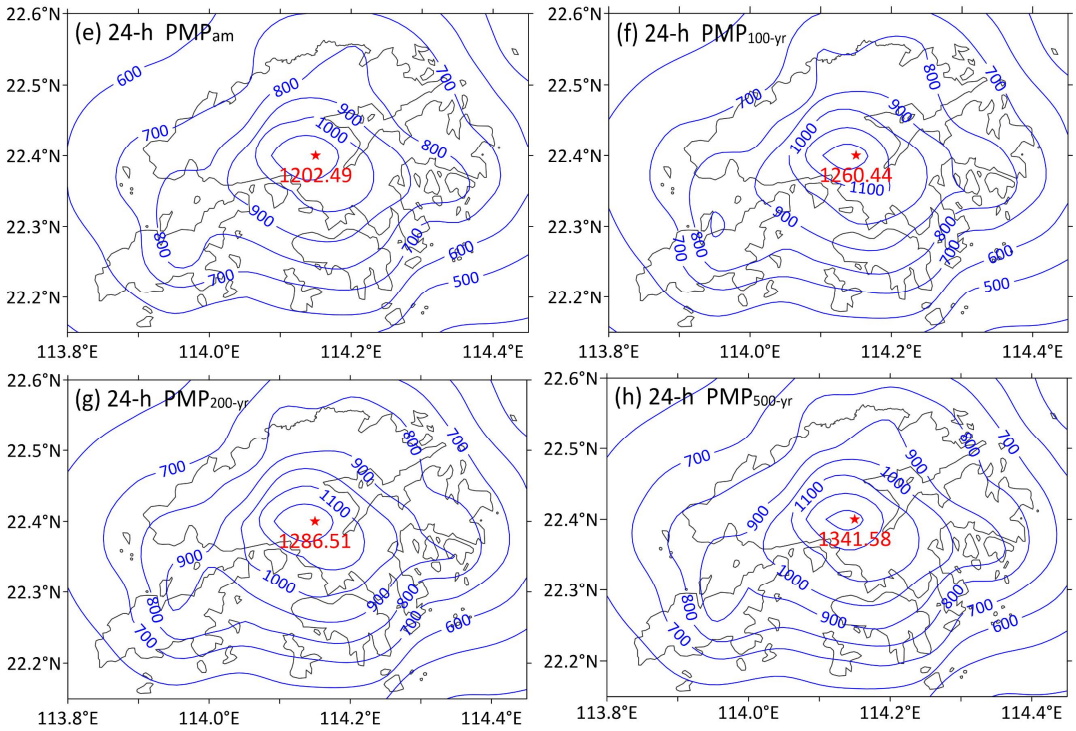

Figure 9. Isohyetal maps of **(a–d)** 4-h and **(e–h)** 24-h Hong Kong embryonic PMP estimates for the cases of (**a**,**e**) annual maximum rainfalls, (**b**,**f**) 100-year rainfall quantiles, (**c**,**g**) 200-year rainfall quantiles, and (**d**,**h**) 500-year rainfall quantiles.

As can be observed from Figure 9, 4-h PMPs estimated based on rainfall quantiles are smaller than PMP_{am}, and along with the increasing return periods, the center values (denoted by red numbers in Figure 9) vary slightly down by about 6%–9% (see Figure 10) for 4-h. While for 24-h, it shows an upper trend and the increasing percentage of $PMP_{500\text{-yr}}$ is up to 11.6%. The decreasing (increasing) variation tendency of center values of 4-h (24-h) PMP is resulting from the increasing (decreasing) trend of 4-h (24-h) OIFs in the center of the convergence rain. The point PMP estimates were compared with the extreme rainfall records in Hong Kong and the world records [28,34,35] to examine their rationality. The point 4-h (24-h) PMPs exceeds the maximum 4-h (24-h) rainfall of 384.0 mm (956.0 mm) recorded at Lantau (Tai Mo Mountain) in Hong Kong but is smaller than the world record. Besides, they are smaller compared to the PMPs estimated by a revised K_m-value method in Hong Kong (i.e., 558.5 mm for 4-h and 1,753.0 mm for 24-h) [49,50]. However, the PMP estimates obtained here so far are actually just embryonic PMPs, so more comparisons should be made after conducting some necessary adjustments such as moisture maximization.

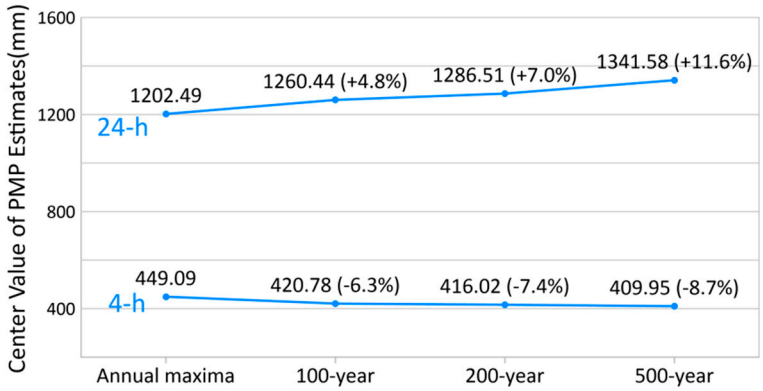

Figure 10. Variation of center values of (**a**) 4-h and (**b**) 24-h Hong Kong PMP based on annual maximum rainfalls, 100-, 200-, and 500-year rainfall quantiles. The percentage variations relative to PMP based on annual maxima are given in parentheses.

5. Summary and Conclusions

In this study, 100-, 200-, and 500-year rainfall quantiles estimated by RLMA were used separately to develop the OIFs of Taiwan under the severe southwesterly moisture inflow, compared with the OIF developed based on annual maximum rainfalls, in the application of SDOIF method for storm separation prior to storm transposition. Then the separated convergence rainfalls were transposed to Hong Kong coupling with the local OIFs for 4- and 24-h PMP. The findings as well as some critical questions that should be analyzed and/or discussed in further studies are summarized as follows:

(1) For 4- and 24-h, there are similar spatial distribution patterns of OIFs on Taiwan Island based on different data samples, which implicates that the SDOIF method is a stable and effective way to separate an orographic component rainfall with spatial distribution from storm rainfalls in mountainous areas.

(2) In general, OIFs obtained based on rainfall quantiles show clearer spatial details of orographic influences on rainfall and better reflect the enhancement effects in orographic intensification areas than that obtained based on annual maxima. Moreover, the separated convergence rainfalls based on rainfall quantiles, which are more accordant with the precipitation purely resulting from atmospheric systems, can be transposed in a larger area. If the convergence rainfalls are transposed and then combined with the local OIFs in design area developed based on local rainfall quantiles, it may get more accurate PMP estimates not only in terms of the center values but also the spatial pattern. Further applications and verifications in other areas with different data should be studied.

(3) For different durations, the center values of OIFs and PMP estimates based on rainfall quantiles may display increasing or decreasing trends with the increase of return periods. Considering quantile estimates may become less accurate and less reliable at larger return periods with respect to the data available, the 100-year rainfall quantiles are recommended most to calculate the OIF in storm separation procedure to achieve more reliable PMP estimates. The accuracy of quantiles estimated via RLMA is influenced by the quality of data (such as number of stations, length of data series) and the validity of delineated homogeneous regions, which will affect the accuracy of OIF values and PMP estimates. If rainfall data with longer time series at more stations are available, a more detailed analysis would be taken to estimate the quantiles, then more accurate and reliable OIFs could be expected.

(4) In SDOIF method, the selection of base stations has an impact on the OIF values. The OIFs computed in this study only represent the topographic effects under the rainfalls with southwesterly moisture jet hitting Taiwan. However, in the cases of estimation for other

areas such as north Taiwan, OIFs under storms with other moisture inflow directions such as northeast or northwest may be applied.

(5) The PMP results in this study are just preliminary PMP estimates that require further adjustments, including transposition adjustments of orientations to the prevailing moisture jet during the invasion of typhoon storms to Hong Kong and moisture maximization.

Author Contributions: Conceptualization, Y.L. and B.L.; data collection, Y.L. and X.C.; formal analysis, Y.L.; software, Y.L., B.L. and H.D.; writing—original draft preparation, Y.L.; writing—review and editing preparation, B.L. All authors have read and agreed to the published version of the manuscript.

Funding: This research was supported by China Institute of Water Resources and Hydropower Research (Grant No. SHZH-IWHR-72), Jiangsu Water Resources Science-Technology Research (Grant No. 2018020), and Civil Engineering and Development Department of Hong Kong Special Administrative Region (Agreement No. CE 13/2011 (GE) and GCST 2/D9/RA 63).

Acknowledgments: The authors would like to thank Taiwan Sinotech Engineering Services, Ltd. and Central Weather Bureau (CWB) of Taiwan for providing the data for research. We would also like to appreciate the editors and the anonymous reviewers for their constructive comments, which helped to improve the quality of this paper.

Conflicts of Interest: The authors declare no conflict of interest.

References

1. World Meteorological Organization. *Manual on Estimation of Probable Maximum Precipitation (PMP)*, 3rd ed.; World Meteorological Organization (WMO): Geneva, Switzerland, 2009.
2. Rakhecha, P.; Clark, C. Revised estimates of one-day probable maximum precipitation (PMP) for India. *Meteorol. Appl.* **1999**, *6*, 343–350. [CrossRef]
3. Australian Bureau of Meteorology. *The Estimation of Probable Maximum Precipitation in Australia: Generalised Short-Duration Method*; Australian Bureau of Meteorology: Sydney, Australia, 2003.
4. Thomas, C.; Golaszewski, R.; Cox, R. Methodology for determining floodway/flow conveyance extent in Australian floodplains. In Proceedings of the Hydrology and Water Resources Symposium (HWRS 2018): Water and Communities, Melbourne, Australia, 3–6 December 2018; Engineers Australia: Melbourne, Australia, 2018; pp. 841–856.
5. Wang, G. *Principles and Methods of PMP/PMF Calculations*; China Water Power Press, Yellow River Conservancy Press: Beijing, China, 1999. (In Chinese)
6. Lin, B. Application of the step-duration orographic intensification factors method to estimation of PMP for mountainous regions. *J. Hohai Univ. Nat. Sci.* **1988**, *16*, 40–52. (In Chinese)
7. Lin, B. Application of the step-duration orographic intensification coefficient method to the estimation of orographic effects on Rainfall. In Proceedings of the Symposium held during the Third Scientific Assembly of the International Association of Hydrological Sciences, Baltimore, MD, USA, 10–19 May 1989; IAHS Publication: Wallingford, UK, 1989; pp. 259–266.
8. Zhang, Y.; Chen, H.; Lan, P. Study on transposition of Taiwan Morakot storm over Hong Kong. *J. Chin. Hydrol.* **2014**, *34*, 25–30. (In Chinese)
9. Bobée, B.; Rasmussen, P.F. Recent advances in flood frequency analysis. *Rev. Geophys.* **1995**, *33*, 1111–1116. [CrossRef]
10. Hosking, J.R.M.; Wallis, J.R. *Regional Frequency Analysis: An Approach Based on L-Moments*; Cambridge University Press: New York, NY, USA, 2005.
11. Dalrymple, T. Flood frequency methods. *USA Geol. Surv. Water Supply Pap. A* **1960**, *1543*, 11–51.
12. Hosking, J.; Wallis, J. Some statistics useful in regional frequency analysis. *Water Resour. Res.* **1993**, *29*, 271–281. [CrossRef]
13. Lin, B.; Bonnin, G.; Martin, D.; Parzybok, T.; Yekta, M.; Riley, D. Regional frequency studies of annual extreme precipitation in the United States based on regional L-moments analysis. In Proceedings of the World Environmental and Water Resource Congress 2006: Examining the Confluence of Environmental and Water Concerns, Omaha, Nebraska, USA, 21–25 May 2006; pp. 1–11.
14. Bonnin, G.; Martin, D.; Lin, B.; Parzybok, T.; Yekta, M.; Riley, D. *Precipitation-Frequency Atlas of the United STATES: NOAA Atlas 14, Volume 1, Version 4*; NOAA, National Weather Service: Silver Spring, MD, USA, 2006.

15. Lin, B. Study and application of hydrometeorological regional L-moments analysis method on flood control standards. In Proceedings of the 2010 Chinese Hydraulic Engineering Society Annual Conference, Guiyang, Guizhou, China, 2–4 November 2010; Yellow River Conservancy Press: Zhengzhou, China, 2010; pp. 261–269. (In Chinese).
16. Wu, J.; Lin, B.; Shao, Y. Application of regional L-moments analysis method in precipitation frequency analysis for Taihu Lake Basin. *J. Chin. Hydrol.* **2015**, *35*, 15–22. (In Chinese)
17. Liang, Y.; Liu, S.; Zhong, G.; Zhou, Z.; Hu, Y. Comparison between conventional moments and L-moments in rainfall frequency analysis for Taihu Lake Basin. *J. Chin. Hydrol.* **2013**, *33*, 16–21. (In Chinese)
18. Fowler, H.; Kilsby, C. A regional frequency analysis of United Kingdom extreme rainfall from 1961 to 2000. *Int. J. Climatol. J. R. Meteorol. Soc.* **2003**, *23*, 1313–1334. [CrossRef]
19. Norbiato, D.; Borga, M.; Sangati, M.; Zanon, F. Regional frequency analysis of extreme precipitation in the eastern Italian Alps and the 29 August 2003 flash flood. *J. Hydrol.* **2007**, *345*, 149–166. [CrossRef]
20. Hailegeorgis, T.T.; Thorolfsson, S.T.; Alfredsen, K. Regional frequency analysis of extreme precipitation with consideration of uncertainties to update IDF curves for the city of Trondheim. *J. Hydrol.* **2013**, *498*, 305–318. [CrossRef]
21. Chen, X.; Lin, B.; Wu, J.; Li, M. Application of hydrometeorological regional L-moments method to storm frequency analysis in Guangxi. *Water Res. Power* **2014**, *32*, 5–9. (In Chinese)
22. Yin, Y.; Chen, H.; Xu, C.-Y.; Xu, W.; Chen, C.; Sun, S. Spatio-temporal characteristics of the extreme precipitation by L-moment-based index-flood method in the Yangtze River Delta region, China. *Theor. Appl. Climatol.* **2016**, *124*, 1005–1022. [CrossRef]
23. Shao, Y.; Wu, J.; Li, M. Frequency analysis of extreme precipitation in Huaihe River Basin based on hydrometeorological regional L-moments method. *J. Chin. Hydrol.* **2016**, *36*, 16–23. (In Chinese)
24. Ding, H.; Liao, Y.; Lin, B. High risk flash flood rainstorm area mapping and its application in Jiangxi Province, China. In Proceedings of the MATEC Web of Conferences, Beijing, China, 16–20 October 2018; EDP Sciences: Les Ulis, France, 2018; p. 01087.
25. Liu, M.; Yin, Y.; Han, C.; Huang, Y. Frequency analysis of extreme precipitation in Jiangxi Province based on regional L-moments method. *Water Res. Power* **2018**, *36*, 1–5. (In Chinese)
26. Li, M.; Ao, T.; Li, X. Regional frequency analysis in hydrological frequency analysis of Sichuan Province. *Southwest Chin. J. Agric. Sci.* **2019**, *32*, 1938–1943. (In Chinese) [CrossRef]
27. Water Resources Agency. *Rainfalls and Inundation during Typhoon Morakot*; Water Resources Agency, MOEA, Taiwan: Taiwan, China, 2009. (In Chinese)
28. Arizona State University. World Meteorological Organization Global Weather & Climate Extremes Archive. Available online: https://wmo.asu.edu/content/world-meteorological-organization-global-weather-climate-extremes-archive (accessed on 25 March 2020).
29. Hong, C.C.; Lee, M.Y.; Hsu, H.H.; Kuo, J.L. Role of submonthly disturbance and 40–50 day ISO on the extreme rainfall event associated with Typhoon Morakot (2009) in southern Taiwan. *Geophys. Res. Lett.* **2010**, *37*, L08805. [CrossRef]
30. Ge, X.; Li, T.; Zhang, S.; Peng, M. What causes the extremely heavy rainfall in Taiwan during Typhoon Morakot (2009)? *Atmos. Sci. Lett.* **2010**, *11*, 46–50. [CrossRef]
31. Wu, L.; Liang, J.; Wu, C.-C. Monsoonal influence on Typhoon Morakot (2009). Part I: Observational analysis. *J. Atmos. Sci.* **2011**, *68*, 2208–2221.
32. Chien, F.C.; Kuo, H.C. On the extreme rainfall of Typhoon Morakot (2009). *J. Geophys. Res. Atmos.* **2011**, *116*, D05104. [CrossRef]
33. Fang, X.; Kuo, Y.-H.; Wang, A. The impacts of Taiwan topography on the predictability of Typhoon Morakot's record-breaking rainfall: A high-resolution ensemble simulation. *Weather Forecast.* **2011**, *26*, 613–633. [CrossRef]
34. AECOM Asia Co. Ltd; Lin, B. *24-h Probable Maximum Precipitation Updating Study*; Geotechnical Engineering Office, Civil Engineering and Development Department, The Government of the Hong Kong Special Administrative Region: Hong Kong, China, 2015.
35. Lin, B. *4-h Probable Maximum Precipitation (PMP) Updating Study in Hong Kong*; Geotechnical Engineering Office, Civil Engineering and Development Department, The Government of the Hong Kong Special Administrative Region: Hong Kong, China, 2017.

36. Chang, W.; Hui, T. Probable maximum precipitation for Hong Kong. In Proceedings of the ATC3 Workshop on Rain-Induced Landslides, Hong Kong, China, 12 December 2001.
37. Greenwood, J.A.; Landwehr, J.M.; Matalas, N.C.; Wallis, J.R. Probability weighted moments: Definition and relation to parameters of several distributions expressable in inverse form. *Water Resour. Res.* **1979**, *15*, 1049–1054. [CrossRef]
38. Hosking, J.R.M. L-moments: Analysis and estimation of distributions using linear combinations of order statistics. *J. R. Stat. Soc. Ser. B Methodol.* **1990**, *52*, 105–124. [CrossRef]
39. Lin, B.; Vogel, J.L. A comparison of L-moments with method of moments. In Proceedings of the Engineering Hydrology, Symposium of American Society of Civil Engineers, ASCE, San Francisco, CA, USA, 25–30 July 1993; pp. 443–448.
40. Wu, C.-C.; Kuo, Y.-H. Typhoons affecting Taiwan: Current understanding and future challenges. *Bull. Am. Meteorol. Soc.* **1999**, *80*, 67–80. [CrossRef]
41. Wu, C.-C. Numerical simulation of Typhoon Gladys (1994) and its interaction with Taiwan terrain using the GFDL hurricane model. *Mon. Weather Rev.* **2001**, *129*, 1533–1549. [CrossRef]
42. Wu, C.-C.; Yen, T.-H.; Kuo, Y.-H.; Wang, W. Rainfall simulation associated with Typhoon Herb (1996) near Taiwan. Part I: The topographic effect. *Weather Forecast.* **2002**, *17*, 1001–1015. [CrossRef]
43. Cheung, K.; Huang, L.-R.; Lee, C.-S. Characteristics of rainfall during tropical cyclone periods in Taiwan. *Nat. Hazards Earth Syst. Sci.* **2008**, *8*, 1463–1474. [CrossRef]
44. Lv, M.; Zou, L.; Yao, M.; Wang, X.; Huang, X. Analysis of asymmetrical structure of precipitation in Typhoon Aere. *J. Trop. Meteorol.* **2009**, *25*, 22–28. (In Chinese)
45. Pan, T.-Y.; Yang, Y.-T.; Kuo, H.-C.; Tan, Y.-C.; Lai, J.-S.; Chang, T.-J.; Lee, C.-S.; Hsu, K.H. Improvement of watershed flood forecasting by typhoon rainfall climate model with an ANN-based southwest monsoon rainfall enhancement. *J. Hydrol.* **2013**, *506*, 90–100. [CrossRef]
46. Wu, W.; Chen, J.; Huang, R. Water budgets of tropical cyclones: Three case studies. *Adv. Atmos. Sci.* **2013**, *30*, 468–484. [CrossRef]
47. Kuo, H.-C.; Chang, C.-P.; Yang, Y.-T.; Chen, Y.-H.; Su, S.-H.; Lin, L.-Y. Large increasing trend of tropical cyclone rainfall in Taiwan and the roles of terrain and southwest monsoon. In *The Global Monsoon System: Research and Forecast*, 3rd ed.; World Scientific: Singapore, 2017; pp. 255–265.
48. Central Weather Bureau of Taiwan. Orders of Meteorological Observation Elements. Available online: https://www.cwb.gov.tw/V8/C/C/Statistics/obsorder.html (accessed on 25 March 2020).
49. Lan, P.; Lin, B.; Chen, X.; Lin, Z. Estimating 4 h PMP in Hong Kong by the improved statistical method and storm transposition. *Water Res. Power* **2018**, *36*, 6–9. (In Chinese)
50. Lan, P.; Lin, B.; Zhang, Y.; Chen, H. Probable maximum precipitation estimation using the revised Km-value method in Hong Kong. *J. Hydrol. Eng.* **2017**, *22*, 05017008. [CrossRef]